Materials Science & Engineering A 655 (2016) 132–141

Contents lists available at ScienceDirect

Materials Science & Engineering A

journal homepage: www.elsevier.com/locate/msea

Thermo-mechanical responses of nanocrystalline Al–Fe alloy processed using mechanical alloying and high frequency heat induction sintering

Muneer Baig [a,*], Hany Rizk Ammar [b], Asiful Hossain Seikh [a]

[a] Advanced Manufacturing Institute-Center of Excellence for Research in Engineering Material, King Saud University, Riyadh, Saudi Arabia
[b] Metallurgical and Materials Engineering Department, Faculty of Petroleum and Mining Engineering, Suez University, Suez, Egypt

ARTICLE INFO

Article history:
Received 15 September 2015
Received in revised form
22 December 2015
Accepted 23 December 2015
Available online 24 December 2015

Keywords:
Nanocrystalline
Al–Fe alloy
Mechanical Alloying
Consolidation
Sintering
XRD
Thermal Stability

ABSTRACT

In the current investigation, a nanocrystalline alloy Al-10 wt.% Fe was synthesized from metallic powders using the mechanical alloying (MA) technique, for various milling hours. The consolidation and sintering of the alloyed powders was performed in a high frequency induction heat sintering (HFIHS) machine. The minimum crystallite size and the maximum hardness of the sintered sample was found to be 30 nm and 2.05 GPa, respectively. The maximum compressive yield strength of the alloy was observed to be 660 MPa at room temperature. The bulk nanocrystalline alloy produced from 150 h milled powder showed significant enhancement in the thermal stability, this specific alloy displayed a compressive yield strength of 570 MPa at 573 K. The compression experimental results of sintered samples revealed high strength coupled with large deformation to failure.

1. Introduction

The demand for aluminum and its alloys has been ever increasing due to their high strength to weight ratio. It is well known that through precipitation hardening mechanisms the strength of certain aluminum alloys at room temperature varies between 550–600 MPa [1]. However, a significant decrease in their strength values with an increase in temperature ($>$ 423 K) has been reported in an earlier investigation [2]. The instantaneous drop in the strength level of the aluminum alloy from room to high temperature has resulted in the limited use of the alloys, especially in high temperature applications. To address this limitation, significant number of investigations were performed, of which few suggested modifications in the manufacturing processes to be implemented in the traditional/or existing processes. A few others suggested alloying of aluminum with transition metals (TM). This suggestion was based to the observations that aluminum when alloyed with TM results in the formation of intermetallics /or secondary phases. These phases tend to provide additional stability to the evolved microstructure and inherently increase the resistance of the alloy against fracture, at higher temperatures [1].

Based on this observation, few investigations have been performed wherein; aluminum was alloyed with TMs for various applications [3–5]. Of the various Al-TMs alloys, Al–Fe alloys is of significant interest owing to the low diffusivity of Fe in aluminum [1,6–9]. The presence of Fe in aluminum matrix results in the formation of stable microstructure of the processed alloy. Fe forms secondary phases with aluminum including their super saturated solution. The microstructural stability of Al–Fe alloys even at elevated temperatures is mainly attributed to the formation of the secondary phases. Thus, it is highly desirable to increase the Fe content in aluminum matrix. However, there exists a solubility limit of Fe in Al matrix if traditional processing methods are employed. The maximum solubility limit of Fe in Al matrix is observed to be less than 0.03 at.% even at elevated temperatures [1] using traditional processing techniques. To enhance the mechanical and physical properties of the Al alloys at elevated temperatures, it is imperative to increase the alloying content of Fe in Al beyond its solubility limit of 0.03 at.%. Due to the limitation of the traditional processing methods, new techniques such as mechanical alloying/milling (MA) [10–13] and rapid solidification (RS) [14,15] can be used. These techniques if carefully implemented tend to increase the solubility limit of Fe in Al matrix. The MA technique is also referred to as non-equilibrium processing technique wherein the alloying process takes place in non-equilibrium condition. Processing of alloys using MA technique not only result in extending the solid solubility limit of Fe in Al matrix but also result in refining the microstructure to ultrafine /or nanometer level with homogeneous dispersion of oxides and intermetallics. Since the alloys produced using these technique consists of higher

* Corresponding author.
E-mail address: bmuneer@ksu.edu.sa (M. Baig).

http://dx.doi.org/10.1016/j.msea.2015.12.077
0921-5093/

content of Fe and refined microstructure, it is expected that the processed alloy shows improved mechanical and physical properties compared to its traditional counterparts [16]. There exists several parameters that define the morphology of final processed powders using MA technique. These parameters include the time and type of mill, milling atmosphere, ball to powder weight ratio, grinding medium and process control agents [13]. MA takes place in a high energy ball mill wherein the powder particles are subjected repetitive welding, fracturing, and re-welding of powder particles resulting in fine particles within a fine grained matrix due to high energy impact [16].

The current study was performed to investigate two aspects. Firstly, to increase the solid solubility limit of TM (Fe) in Al matrix and secondly, to investigate the mechanical properties of the processed alloy at elevated temperatures. The current investigation further explores the synergistic effect of increasing the alloying time and the reduction in the crystallite size of the processed alloy, on the thermo-mechanical properties of the sintered alloy which has not been fully explored in earlier investigations.

2. Experimental procedure

2.1. Production of ultrafine/nanocrystalline Al -10%Fe alloys

The initial powders used in this investigation include; 99.95% pure Al powders (average particle size equal to 2 μm) and 99.95% pure Fe powders (average particle size equal to 3 μm). In order to remove any traces of moisture present in the initial powders, the mixture (consisting of Al-10 wt.% Fe powder) was degassed in vacuum oven at 373 K for 24 h. The degassed mixture was charged into the milling containers along with steel balls of 15 mm diameter in a glove box under inert atmosphere. The number of balls in each container was selected so that the ball-to-powder weight ratio (BPR) of 10:1 was maintained. The MA of charged powders was performed in a pulverisette-P5 planetary ball mill with a milling speed of 120 rpm. To understand the effect of milling time on the severity of alloying, the milling times performed in this investigation include 10, 30, 70, 100 and 150 h. To avoid excessive heating of powders each milling cycle consisted of 15 min of milling alternated with 15 min of pause time. Processing of powders using MA could lead to a significant agglomeration of powder particles due to the repeated cold welding, fracture and re-welding [13]. Thus, to inhibit the agglomeration of the powder particles during alloying, various process control agents (PCA) are normally used [12,17,18]. In the current investigation, 1 wt.% stearic acid was used as a process control agent (PCA). After milling, the milled mixture was charged into a graphite mold in a glove box maintained under inert atmosphere. To ensure inert atmosphere while transferring the mold from glove box to sintering machine, the top and bottom surface of the charged powder was covered with a thin layer of graphite powder. The powders in the mold were then consolidated and sintered in a HFIHS machine under vacuum to form bulk nanocrystalline alloy. The rate of heating and the sintering temperature were set to 823 K/minute and 823 K, respectively. Once the desired temperature of 823 K was reached, the sintering was performed for an additional 6 minutes, while maintaining a constant pressure of 50 MPa. The density of the sintered bulk nanocrystalline alloy was measured using Sartorius density measurement kit and the bulk density of the sintered alloy was found to be 2.84 g/cm^3.

2.2. Vickers microhardness

The Vickers microhardness measurements were performed on the sintered Al-10 wt.% Fe alloy obtained from milled powders for various milling times, using Buehler microhardness tester. The load for the indentation was set to 100 g. The surface of the samples were polished using sand papers of different grits. The different grit sizes used range from 220 to 4000. The final polishing was performed using a colloidal silica solution. The measurements were performed at an interval of 0.25 mm along the sample diameter.

2.3. Compression experiments at room temperature

The quasi-static uniaxial room temperature compression experiments were performed on the sintered Al-10 wt.% Fe alloy samples, at a constant engineering strain-rate of $10^{-2}\,s^{-1}$ on an Instron material testing system. The typical specimen dimensions include 13 mm length and 9 mm diameter. To maintain a constant engineering strain-rate during the experiment, the samples were experimented in the displacement-controlled mode. A uniaxial high elongation strain gage manufactured by Kyowa was bonded on the sample surface. The strain gage was connected to P3500 strain indicator manufactured by Vishay micro measurements. The reading obtained from strain indicator was later corrected using calibration factor to obtain strain. The stress was calculated from the load values obtained from load transducer. It is well known that the friction plays a significant role in the compression experiments. To negate the friction effects, the interface between the surface's of the test specimen and machine grips was lubricated with a combination of a Teflon sheet of 0.3 mm thickness and Molycote grease.

2.4. Quasi static compression experiments at different temperatures

To investigate the effect of temperature on the mechanical responses of sintered Al-10 wt.% Fe alloy, the samples were subjected to compressive loading at a strain-rate of $10^{-2}\,s^{-1}$ and at temperatures of 373 K, 473 K and 573 K. The displacement from the machine transducer was corrected for the machine compliance. The corrected displacement data was used to calculate the strain. High temperature grease manufactured by Dow Corning was used as a lubricant. The thermocouple (Type J) mounted on the surface of the specimen provided the temperature reading. Before performing the experiment, the specimen was heated to the desired temperature and held at that temperature for additional 15 minutes to obtain the uniformity of the temperature throughout the specimen.

2.5. X-Ray diffraction

The surfaces of newly fabricated nanocrystalline Al-10 wt.% Fe bulk sample was mirror polished using various grit sand papers starting with a coarse paper and ending with fine polishing using colloidal silica solution. The polished surface of the sample was characterized on a Discover D8 diffractometer operating in the θ–θ geometry using a standard Cu-K_α (λ=0.154 nm) radiation. The sample surface was scanned at a rate of 5° per minute for a 2θ value between 30 and 50 degree. This 2θ range was sufficient enough to record the first two peaks of Al. The maximum intensity peak obtained from (1 1 1) diffraction plane of Al was used to calculate the average grain (crystallite) size using Debye-Scherrer's [19] equation given by

$$D = \frac{K\lambda}{B\,\mathrm{Cos}\,\theta} \tag{1}$$

where, D, K, λ, B and θ represents the crystallite size, shape factor (assumed to be 0.9), wavelength (0.154 nm) of Cu-K_α radiation, full width at half maximum (in radians) and the peak position, respectively.

2.6. Scanning and Transmission Electron Microscopy

JEOL model JSM-6610LV FESEM with an energy dispersive X-ray analyzer and JEM-2100F HRTEM were used for characterizing the microstructural constituents and features of the as-mixed, milled and sintered samples. The powder samples for TEM analysis were prepared by dissolving small quantity of the powder in an ethanol solution. The solution was sonicated for 1 h using a probe sonicator. A drop of sonicated solution was dispersed on silicon wafer and dried to evaporate the solution leaving behind the sintered powder on the silicon grid.

3. Results and discussion

Fig. 1a shows the morphology of the as-mixed powder containing a mixture of Al-10 wt.% Fe. The initial as-mixed powders appeared to be spherical shaped having an average particle size in the range of the 2–4 μm. Fig. 1b–f show the morphology of the processed powders milled for various milling hours. The powders milled to 70 or greater than 70 h were in the form of flakes. During milling the particles are repeatedly flattened, cold welded, fractured and re-welded resulting in significant straining of the powder particles. The change in the morphology of the milled

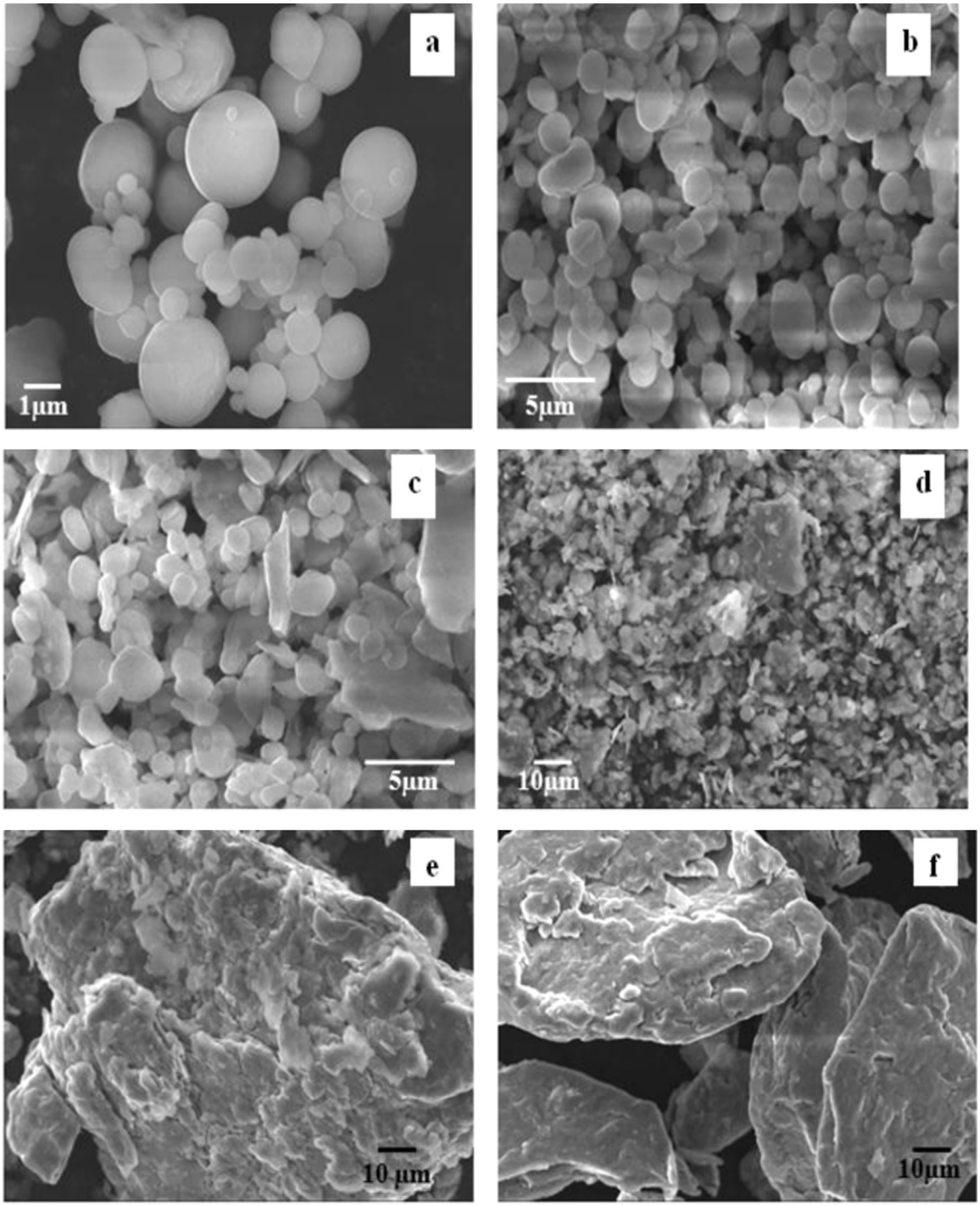

Fig. 1. SEM images of the Al-10 wt.% Fe alloy powders (a) as-mixed (b) 10 h (c) 30 h (d) 70 h (e) 100 h and (f) 150 h.

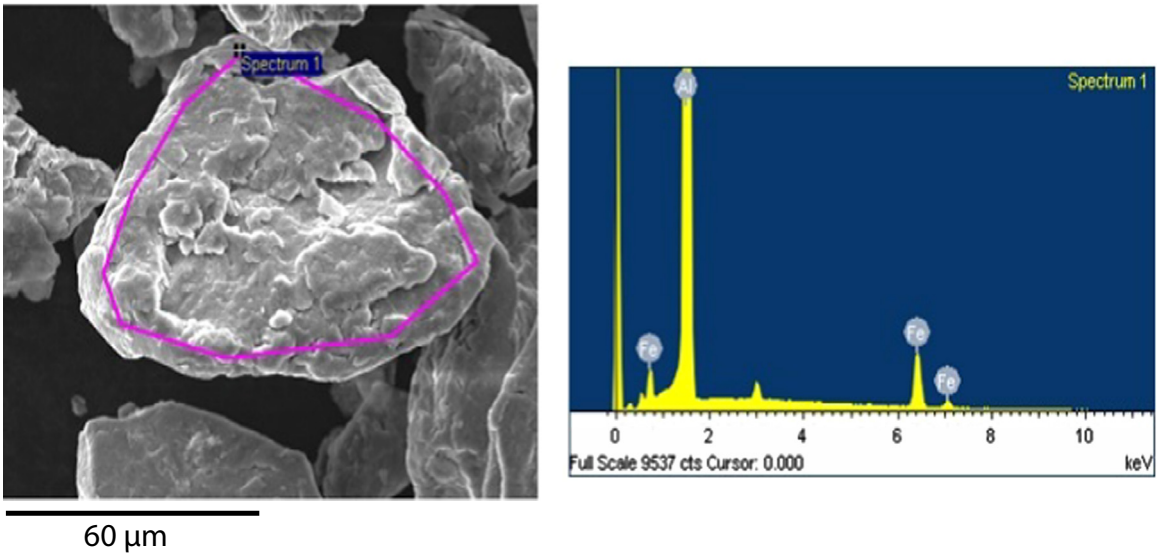

Fig. 2. Image from SEM and EDX of 150 h milled powders.

powder from spherical to flakes could be attributed to the large amount of straining that takes place during the milling. It may be observed from Fig. 1 d–f that, 1 wt.% of stearic acid (PCA) used in this investigation was insufficient to inhibit agglomeration of the milled powders as suggested in the literature [13]. A higher percentage of around 3–5% PCA will be optimum for processing such kinds of alloys.

Fig. 2 shows the results from the SEM-EDX analysis of a powder particle obtained from the 150 h milled powder. Form the EDX spectrum; it is evident that the selected particle consists of elements such as Al and Fe. The weight percent of Al and Fe was found to be 89% and 11%, respectively. A slight increase in the alloying content could be expected due to the contamination during milling, especially for long hours.

Fig. 3 shows the XRD spectrum of the as-received and milled powders. The diffraction peaks were observed to be that of Al and Fe. From the figure, the shifting of Al peaks with milling time to a higher diffraction angle is observed. The shifting of peaks shown in Table 1, suggests that the MA lead to the dissolution of Fe in the Al matrix. This evidence is supported from the results of EDX shown in Fig. 2, which indicates the presence of Fe in the processed alloy. A further analysis of XRD spectrum of the processed powders did not reveal significant information related to the formation of new phases. However, it could be interpreted that the alloying of 10 wt.

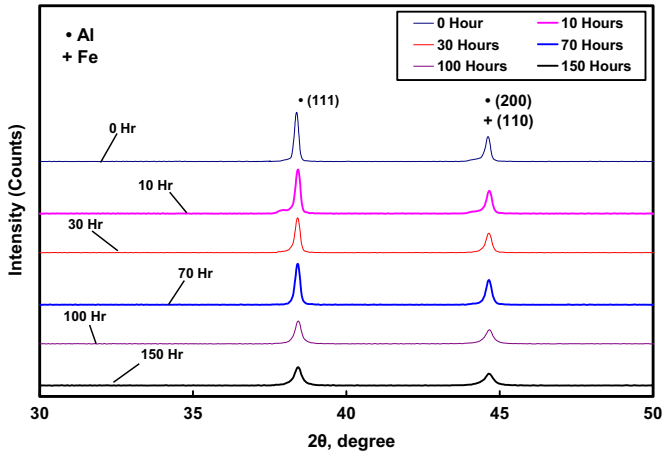

Fig. 3. XRD spectrum of the as received (0 h) and milled powders for different milling times.

Table 1
The measured 2θ and B values of the as-received and milled powders for different milling times.

Milling Time (Hours)	Measured 2θ for Al peak (111) plane (deg)	Measured B for Al peak (111) plane (deg)
0	38.3817	0.1631
10	38.4135	0.1834
30	38.4214	0.1933
70	38.4257	0.2039
100	38.4301	0.2467
150	38.4354	0.2854

% Fe with Al resulted in the formation of supersaturated solid solution (SSSS). Thus, it can be inferred that the solid solubility limit of Fe in Al matrix was successfully increased to 10 wt.% using MA.

In the present investigation, aluminum was successfully alloyed with 10 wt.% of Fe to form a supersaturated solid solution as opposed to a maximum equilibrium solubility limit of 0.03 at.% using other conventional methods [20]. From the Fig. 3, it is observed that an increase in milling time resulted in the broadening of the Al peaks along with a reduction in peak intensities. This indicates the crystal refinement along with accumulation of lattice strain as a result of MA.

Table 2, shows the variation in calculated values of crystallite size and lattice parameter with milling time. It is evident that the crystallite size decreases with an increase in milling time. The most intensive Al peak (111) from the XRD spectrum was used to obtain the crystallite size and lattice parameter. It is observed that the crystallite size decreased gradually with an increase in milling time. The average crystallite size for the 150 h milled powders was found to be 30 nm. Also, it is observed that the lattice parameter decreases with an increase in milling time providing an evidence

Table 2
Variation in the crystallite size and lattice parameter of alloyed powders.

Time of Alloying (Hrs)	Crystallite Size (nm)	Lattice Parameter (nm)
10	45.8694	0.40559
30	43.5217	0.40548
70	41.2597	0.40543
100	34.1021	0.40539
150	29.4783	0.40534

for the dissolution of more Fe into the alloy with increasing milling times.

The above-mentioned XRD results of the milled powders confirmed the formation of Al–Fe alloy in the form of solid solution as a consequence of mechanical milling. Several studies [9,21,22] reported that the shift in A1 peaks to higher angles and the decrease in the lattice parameter of Al are strong evidences for the formation of Al–Fe solid solution which are in a complete agreement with the results obtained in the current study. Furthermore, in the present study, the amount of iron added (10 wt.% ≈ 5 at.%) to form a solid solution with Al matches the reported values of 1–4.5 at.% Fe that can be completely dissolve in Al using mechanical alloying [9,21,22].

The results presented in Figs. 1 through 3 are in a full agreement with the assumptions given for the mechanisms of mechanical alloying and extension of solid solubility limit [13]. During the process of mechanical milling, the powder particles are subjected to a heavy plastic deformation. As a consequence, a diversity of crystalline imperfections are introduced to the metal powders, these include vacancies, dislocations, stacking faults, and increased number of grain boundaries. These imperfections improves the diffusivity of Fe atoms into the Al matrix. Additionally, the diffusion path decreases as a result of the refinement of the microstructural constituents down to the nanoscale. Furthermore, the heat generated during mechanical milling process aids the atomic diffusion. The large volume fraction of atoms in the grain boundaries in such nanocrystalline alloys is expected to further enhance atomic diffusion and consequently extending the solubility limit of Fe in Al. Under the previously mentioned conditions, during mechanical alloying process, a rapid atomic diffusion dominants and results in homogenizing the structure and ultimately forming the Al–Fe solid solution in the processed powders.

Fig. 4 shows the SEM backscattered images of the Al-10 wt.% Fe powder annealed in vacuum at 823 K for 6 min, a condition similar to sintering except the absence of pressure (or pressure less sintering). Fig. 4(a) shows the SEM image of the annealed powder. Fig. 4(b) shows the contrast SEM image showing the distribution of Al matrix. The bright area in the figure corresponds to the α-Al phase and the dark area corresponds to the α-Fe phase. Similarly, the bright area shown in Fig. 4(c) corresponds to the α-Fe phase and the dark area represents α-Al phase. From the figure, it is evident that 150 h of milling resulted in complete and homogeneous dispersion of Fe in Al matrix.

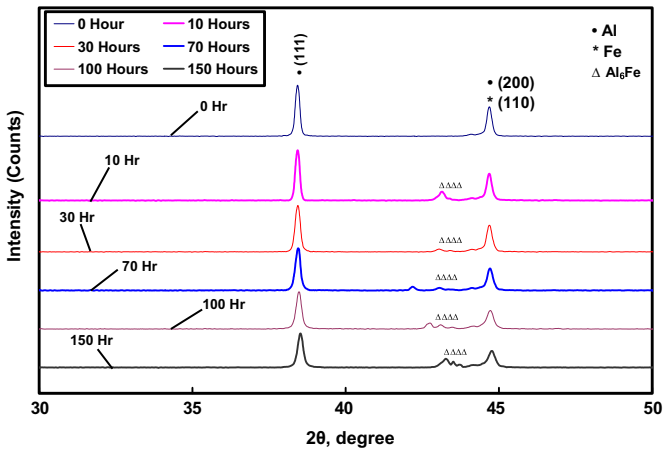

Fig. 5. XRD spectrum of the sintered samples obtained from as received (0 h) and milled powders for different milling times.

The XRD spectrum of the sintered Al-10 wt.% Fe alloy for different milling times is shown in Fig. 5. The measured values of 2θ and B for the sintered samples are shown in Table 3.

It is observed that during sintering, the Fe is precipitated from

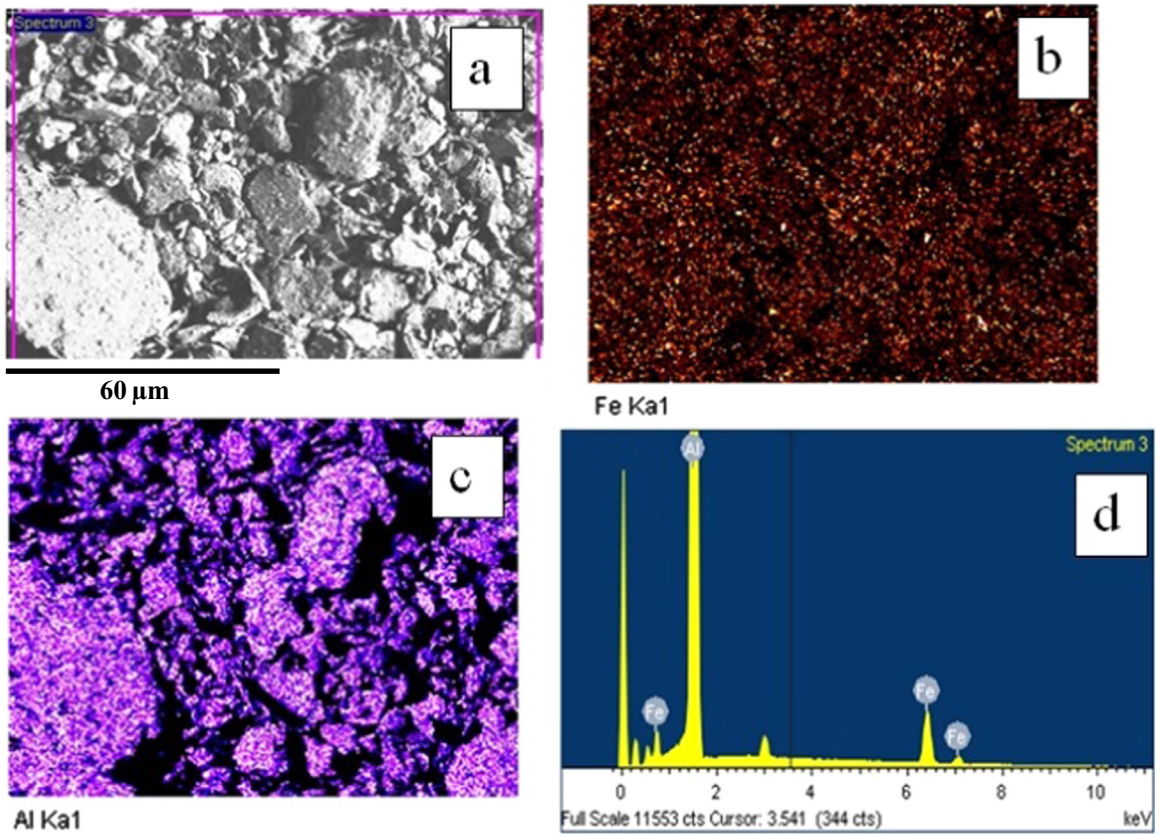

Fig. 4. SEM backscattered image along with EDX of the Al-10 wt.% Fe powder annealed in vacuum at 823 K for 6 min.

Table 3
The measured 2θ and B values of the as-received and sintered samples for different milling times.

Milling Time (Hours)	Measured 2θ for Al peak (111) plane (deg)	Measured B for Al peak (111) plane (deg)
0	38.4313	0.1669
10	38.4353	0.1714
30	38.4415	0.1751
70	38.4557	0.1985
100	38.4815	0.2138
150	38.5273	0.2243

the supersaturated Al–Fe solid solution to form a metastable intermetallic Al_6Fe phase. Similar observations were reported in earlier investigations [6,9,22]. However, in some studies the sintered alloy was further annealed prior to XRD analysis. In the current investigation, the sintered alloy showed the precipitation of Fe without further annealing. This is directly related to the thermal cycle involved during sintering process which includes heating rate of 823 K/min to reach the designated sintering temperature of 823 K for 6 min, at this temperature Al–Fe exists in the form of supersaturated solid solution, once sintering time is completed, the alloy is cooled from sintering to room temperature with a specific cooling rate, during cooling of the sintered sample, Fe atoms precipitates out of the solid solution and form the Al_6Fe intermetallic phase in the matrix.

Table 4, shows the variation in the crystallite size and lattice parameter with milling time of the sintered samples. On comparing the results from Table 2 with Table 4, the crystallite size of 150 h milled powder and sintered alloy was found to be 30 nm and 38 nm, respectively.

It is well known that the crystallite size of the powders increase during sintering process because of the involvement of high temperature which support the grain growth mechanism. However, the change in crystallite size was observed to be minimal in this investigation as shown in Table 4 and could be due to the rapid heating rate (550 °C/min) and short holding time (6 min) followed in the current investigation using HFIHS technique. The rapid rate of heating and short holding time of sintering results in restricting the grain growth mechanism since the time of the sintering process is too short to support a considerable change in the crystallite size.

Fig. 6 shows the plot of difference in crystallite size (DCS) and lattice parameter (DLP) with milling time. The DCS and DLP were calculated as follows:

$$\text{DCS} = \text{Crystallite size (sintered alloy)} - \text{Crystallite size (powder)} \quad (2)$$

$$\text{DLP} = \text{Lattice parameter (powder)} - \text{Lattice parameter (sintered alloy)} \quad (3)$$

The maximum difference in lattice parameter (DLP) after sintering is observed in samples obtained from 150 h milled powders. This observation implies that during the sintering of 150 h milled

Table 4
Variation in the crystallite size and lattice parameter of the sintered samples.

Time of Alloying (Hrs)	Crystallite Size (nm)	Lattice Parameter (nm)
10	49.0847	0.40534
30	48.0482	0.40529
70	42.386	0.40513
100	39.3557	0.40488
150	37.5188	0.40441

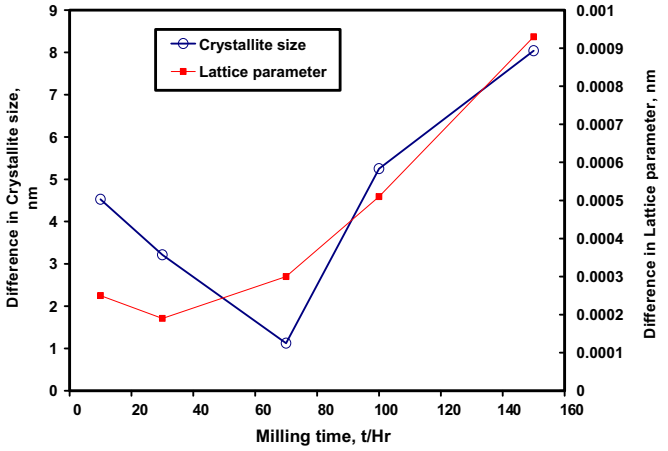

Fig. 6. The crystallite size and lattice parameter variation after sintering with the milling time.

powder, the precipitation of Fe atoms from the SSSS is maximum and consequently could possess maximum content of metastable Al_6Fe intermetallic. Thus, Al–Fe alloy produced from 150 h milled powder is expected to exhibit highest thermal stability and consequently, the alloys produced from 10 h and 30 h milled powder is expected to exhibit the least thermal stability.

Fig. 7 shows the SEM backscattered image of the sintered Al-10 wt.% Fe alloy obtained from 150 h milled powders. Fig. 7 (a) shows the SEM image of the alloy surface. Fig. 7(b) shows the contrast SEM image showing the dispersion of Al matrix. The bright area corresponds to the Fe-containing phases and the dark area corresponds to the Al matrix. Similarly, the bright area in Fig. 7(c) corresponds to the Al matrix and the dark area corresponds to the Fe-containing phases. The SEM-EDX analysis of the sample surface in Fig. 7(a) is shown in Fig. 7(d). From the Fig. 7(d), it is evident that the EDX detected Al and Fe as the major constituents, indicating that the grain refinement process followed in the current investigation did not introduce any other contamination.

Fig. 8 shows the high resolution image of the sintered powder (after 150 h of milling) sample obtained from HRTEM. From the figure, it is observed that the sintered powder sample consists of nanocrystalline (n.c) Al and the metastable Al_6Fe phase. The inserts on top of the figure shows the SAD pattern for the n.c Al and Al_6Fe phase. The dispersion of the metastable phase was observed to be homogeneous in the n.c Al matrix. The presence of this metastable phase in the Al matrix is responsible for providing the microstructural stability to the alloy at elevated temperatures.

The Fig. 9(a) shows the bright-field image of the sintered powder. The microstructure of the powder is observed to consist of nanocrystalline grains. The indexing of selected area diffraction (SAD) pattern indicated the presence of metastable Al_6Fe phase in the microstructure of the sintered alloy. This further confirms with the results obtained using the XRD profiles indicating the presence of metastable phase in the sintered alloy. Also, the presence of sharp rings in the SAD pattern confirms the crystallinity of the sintered alloy and indicates the presence of nanocrystalline particles. The dark-field image shown in Fig. 9(b) was obtained by exciting the (111) reflection of Al and is observed to be composed of nanocrystalline grains.

Fig. 10 shows the hardness distribution profiles on the surface of sintered Al-10 wt.% Fe alloy for various milling times. It is observed that the hardness increases with an increase in milling time. It is also observed that the sintered alloy obtained from 10 and 30 h milled powder showed larger variation in the measured hardness along the surface. This could be due to the fact that at

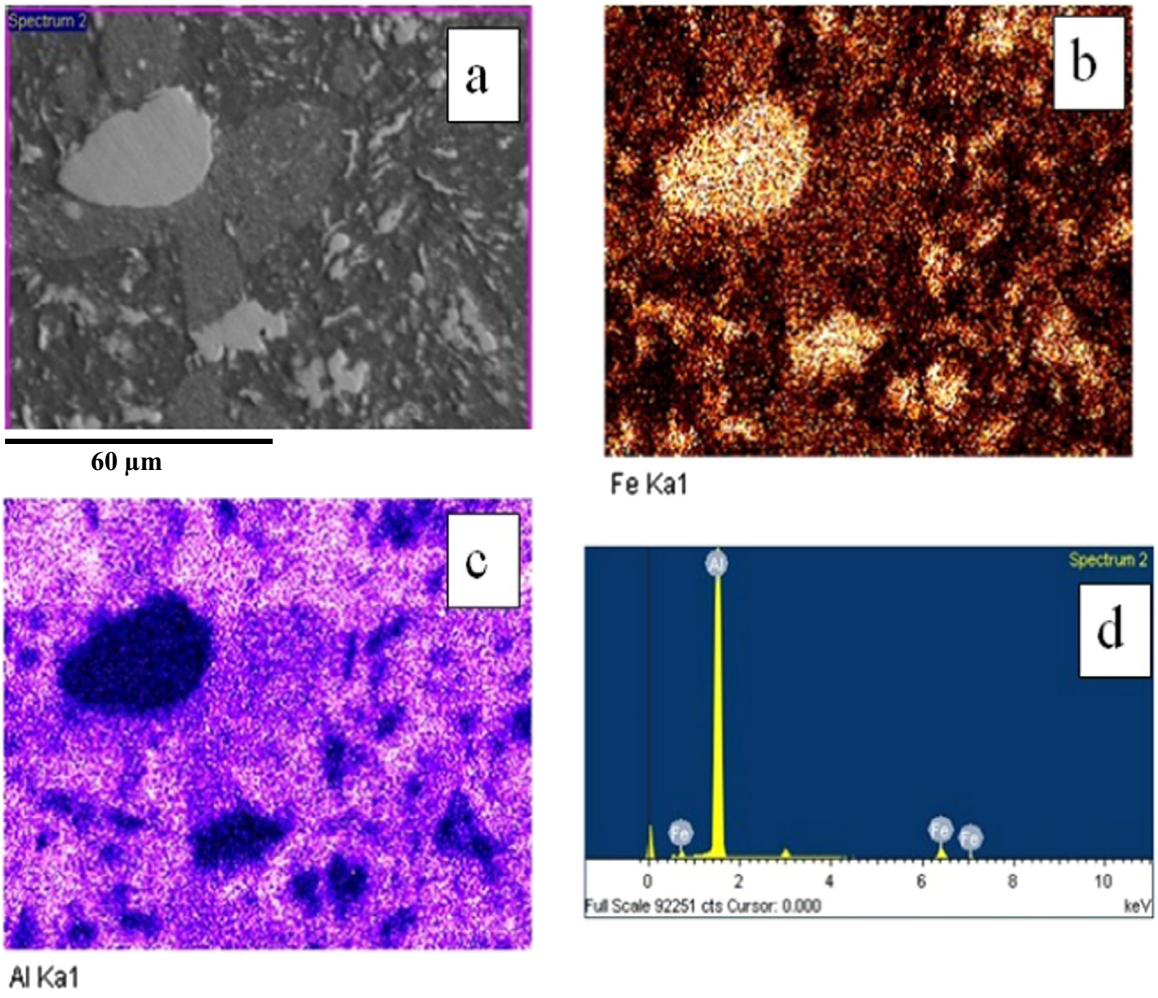

Fig. 7. SEM image mapping of the sintered sample obtained from 150 h milled powder.

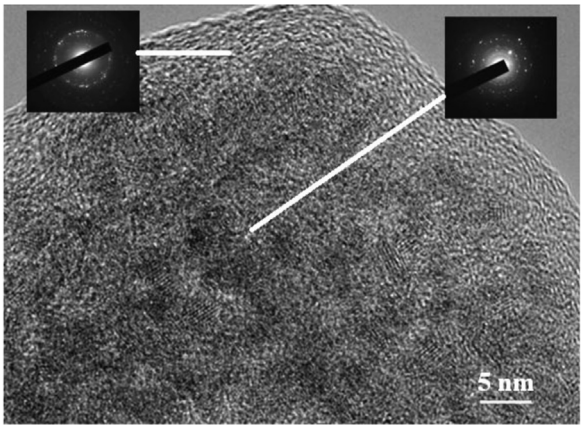

Fig. 8. High resolution image of the sintered powder (after 150 h of milling) sample obtained from HRTEM.

lower milling times, the distribution of Fe atoms in the Al matrix is not homogenous. However, the surface hardness values were observed to stabilize in samples obtained from powders milled for more than 70 h. This observation could be attributed to the homogeneous dispersion of Fe atoms in the alloy which tend to increase with an increase in milling time. This implies that samples produced from powders, processed by MA for longer hours could exhibit similar properties throughout the specimen. A maximum hardness value of 2.05 GPa was observed in the alloy produced from 150 h milled powders. This hardness value is considered extremely high, as compared to conventional Al alloys. The significantly increased hardness in this condition is related to the effect of several hardening mechanism in the processed alloy [6,23]. These include: solid solution strengthening, ultrafine/nanoscale crystallites size, dispersion hardening of Al matrix by the ultrafine/nanoscale Al_6Fe intermetallic, and the introduction of numerous crystalline imperfections to the alloy structure during the powders processing.

Fig. 11 shows the compressive true stress–strain experimental responses of Al-10 wt.% Fe alloy obtained from sintering of 10 h milled powder. The sintered alloy exhibited considerable work hardening behavior. However, the work hardening response of the alloy diminished with an increase in temperature. The room and high temperature yield strength was found to be between 288 and 165 MPa, respectively.

Fig. 12 shows the true stress–strain experimental responses of Al-10 wt.% Fe alloy obtained from sintering of 30 h milled powder. It is observed that the room temperature yield stress of alloy increased marginally when compared to results from Fig. 11. However, the temperature stability was observed to be slightly better than the alloy obtained from 10 h milled powder.

Fig. 13 shows the experimental responses of Al-10 wt.% Fe alloy sintered from 70 h milled powders. It is observed that increasing milling time resulted in an increase in the overall yield stress of the material. Also, the room temperature work hardening behavior tends to diminish with increasing milling time.

Fig. 14 shows the responses of Al-10 wt.% Fe alloy sintered from

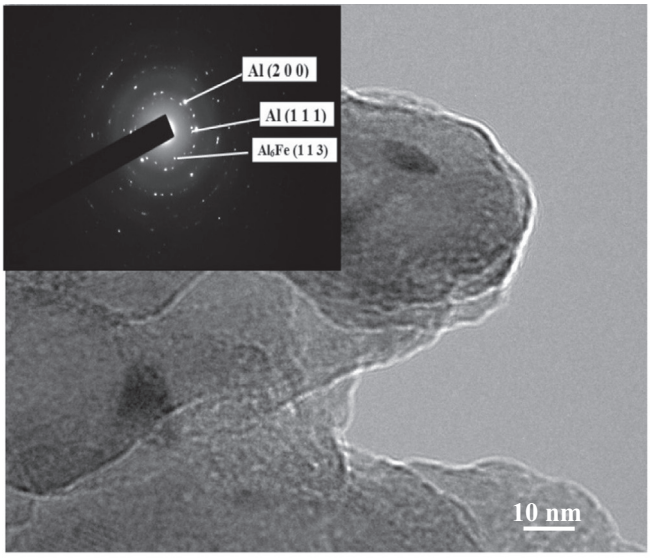

(a)

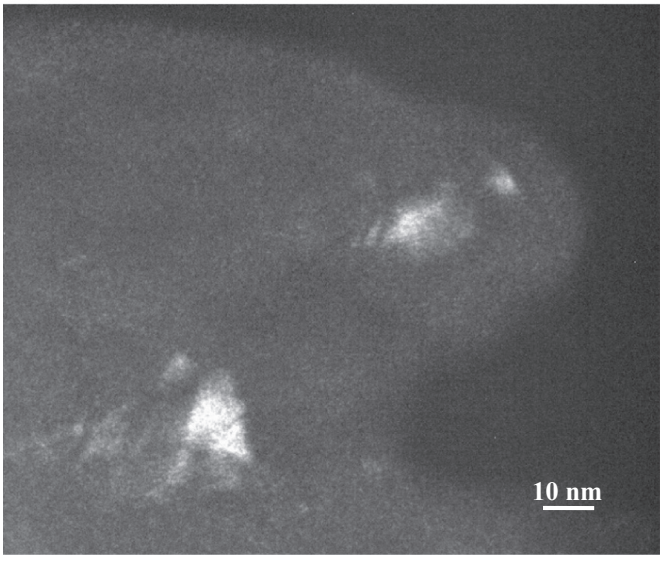

(b)

Fig. 9. TEM micrographs of the sintered powder after 150 h of milling; (a) bright-field TEM image with embedded SAD pattern and (b) dark field TEM image obtained using Al (111) reflection.

100 h milled powders. It is observed that the room temperature yield stress of the sintered sample increased to 550 MPa after 100 h of milling compared to 271 MPa exhibited by 10 h milled powder. As observed from the figure, the mechanical properties of samples obtained from 100 h milled powder showed enhanced thermal stability.

Fig. 15 shows the true stress–strain experimental responses of Al-10 wt.% Fe alloy obtained from sintering of 150 h milled powder. The room temperature yield stress was found to be 636 MPa while the yield strength at 573 K was observed to be 571 MPa. As expected, the sintered alloy from 150 h milled powder showed a significant increase in the yield stress along with superior thermal stability which is related to smallest crystallite size obtained; the increased solubility limit of Fe in Al. The increase in solubility of Fe implies the formation of large volume fraction of Fe-containing intermetallic phases. These intermetallics tend to provide microstructural stability at high temperatures, results in improved

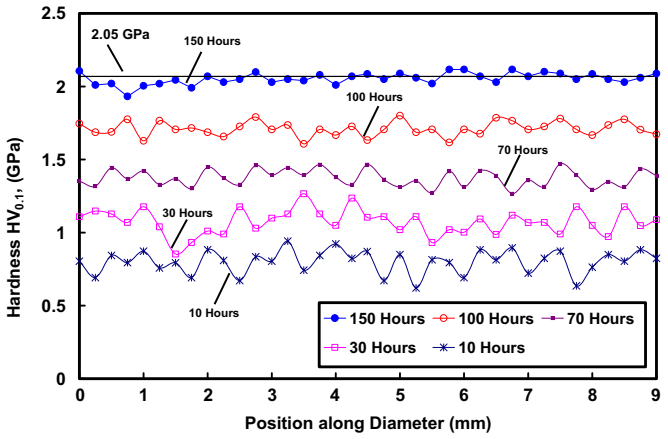

Fig. 10. Hardness variation along the diameter on the surface of sintered samples obtained from powders of different milling times.

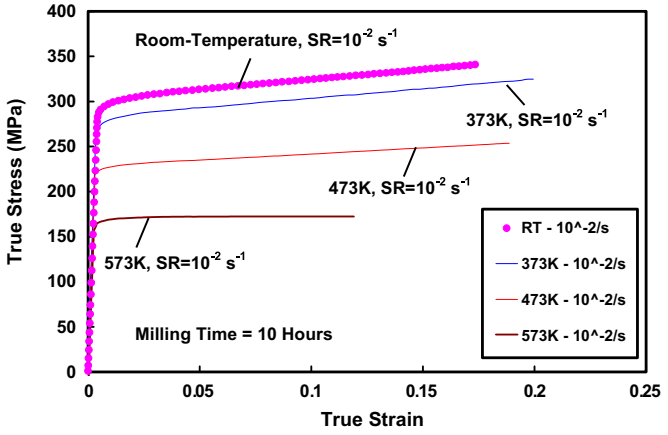

Fig. 11. True compressive stress–strain response of the sintered sample obtained from 10 h milled powders.

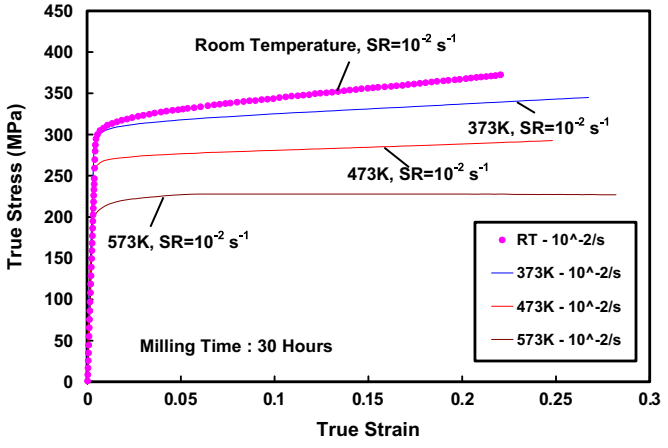

Fig. 12. True compressive stress–strain response of the sintered sample obtained from 30 h milled powders.

mechanical properties at elevated temperatures. From the Figs. 11–15 it is observed that with increasing milling time, the strength of the processed alloy increases which is related to the fact that several strengthening mechanisms become effective, as mentioned earlier in this section. This strengthening effect, however, takes place at the expense of alloy ductility, as may be observed in Figs 11–15, the alloy ductility decreases with increasing milling time.

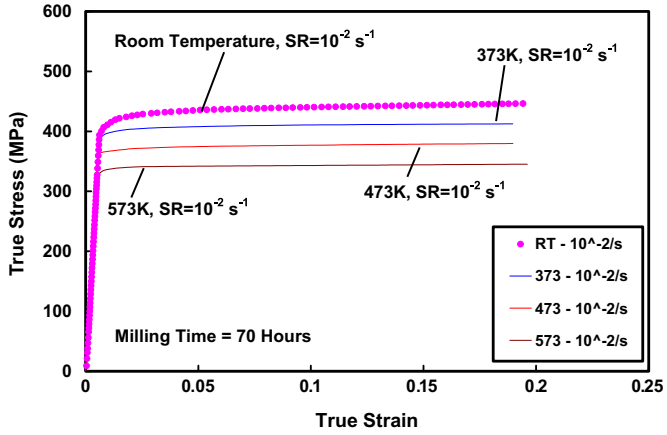

Fig. 13. True compressive stress–strain response of the sintered sample obtained from 70 h milled powders.

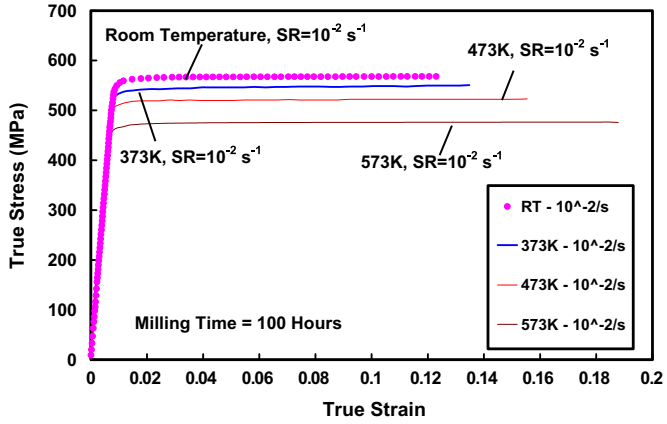

Fig. 14. True compressive stress–strain response of the sintered sample obtained from 100 h milled powders.

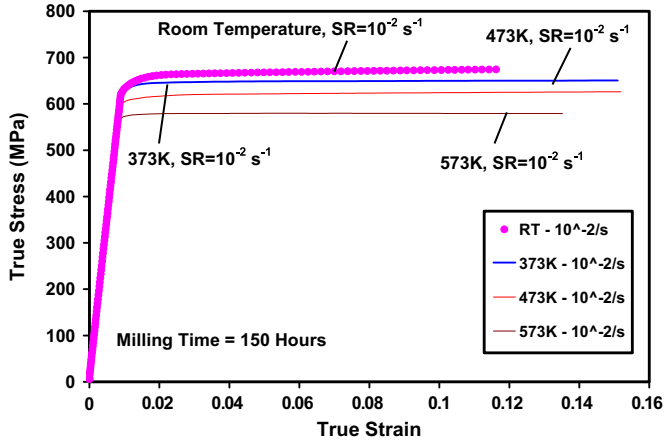

Fig. 15. True compressive stress–strain response of the sintered sample obtained from 150 h milled powders.

Fig. 16 shows the variation in the yield stress with temperature for the sintered alloys obtained from 10, 30, 70, 100 and 150 h milled powders. It is observed that the yield stress of the sintered alloy varies non-linearly with temperature. Also, decrease in the yield stress with temperature was found to be 65 MPa for sintered samples obtained from 150 h milled powders signifying better thermal stability as oppose to a drop of 123 and 76 MPa in the yield stress for 10 and 70 h milled powders, respectively.

Thus, it is evident that samples obtained from 150 h milled

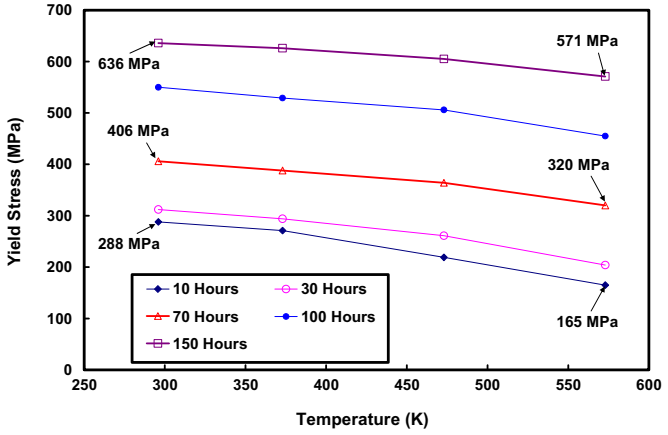

Fig. 16. Variation in the yield stress of the sintered samples with temperature for different milling times.

powder exhibited higher yield strength, better thermal stability and increased strain-rate sensitivity. The enhancement in the mechanical properties with milling time is attributed to the extension of solubility limit which allow more iron to dissolve in the Al-matrix; the refinement of the microstructure into nanoscale; and the formation of thermally stable Fe-containing phases with ultrafine size such as Al_6Fe. The thermal stability of the alloy milled for 150 h could be attributed to the fact that, the extremely long hours of milling time provided the maximum amount of Fe in Al matrix as a solid solution and also will produce the maximum amount of intermetallics. The formation of Al_6Fe dispersoids hinder the diffusion of Fe in Al, in addition to the low diffusivity of iron in aluminum even at elevated temperature, this explains the main reasons behind the high yield strength of 571 MPa obtained at 573 K, the microstructure of the alloy is thermally stable and retain its main characteristics obtained from processing even at this elevated temperature. These observations are in a total agreement with reported results of other studies on Al–Fe alloys processed by mechanical alloying [1,9,24].

4. Conclusions

Nanocrystalline Al-10 wt.% Fe alloy was sintered from the milled powders subjected to different milling times. The milled powders and their sintered alloy were characterized using XRD to predict the presence of different phases. The milled powder showed the dissolution of Fe in Al and is confirmed by XRD peak broadening and shifting for all milling times. This indicates the formation of SSSS of Fe in Al. It is observed that, higher milling times resulted in higher dissolution and dispersion of Fe particles in Al matrix. The HRTEM along with XRD profiles provided the evidence for the formation of metastable phases after sintering. The lattice parameter was observed to decrease with increase in milling time indicating the dissolution of more Fe with milling time. However, after sintering, Al_6Fe intermetallic precipitated in the microstructure of the alloy. The presence of intermetallic imparted thermal stability to the alloy, as observed from the results of compression experiments. It is concluded that the addition of Fe in the current investigation has resulted in establishing the microstructural stability of the Al alloy. The Vickers microhardness measurements obtained from 150 h milled powder showed a high value of 2.05 GPa at room temperature. The bulk samples obtained from the milled (for 150 h) powders displayed maximum thermal stability, where the room temperature strength was observed to be 660 MPa and the yield strength at 573 K was 570 MPa. The sintered alloy exhibited large strain to failure indicating the

homogeneity of the processed alloys. The work hardening of the alloy was observed to decrease with increasing milling time.

Acknowledgement

This project was funded by the National Plan for Science, Technology and Innovation (MAARIFAH), King Abdulaziz City for Science and Technology, Kingdom of Saudi Arabia, Award Number (12-NAN2635-02).

References

[1] T. Sasaki, T. Mukai, K. Hono, A high-strength bulk nanocrystalline Al–Fe alloy processed by mechanical alloying and spark plasma sintering, Scr. Mater. 57 (2007) 189–192.
[2] A.S. Khan, M. Baig, Anisotropic responses, constitutive modeling and the effects of strain-rate and temperature on the formability of an aluminum alloy, Int. J. Plast. 27 (2011) 522–538.
[3] F.H. Sanchez, F. Namavar, J.I. Budnick, A. Fasihuddin, C.H. Koch, H.C. Hayden, Effect of temperature on high fluence transition metal implants into polycrystalline aluminum, Mater. Sci. Eng. 90 (1987) 149–159.
[4] A.E. Kiv, V.I. Ezersky, M.M. Talianker, The stability of structures with icosahedral local order in Al-based alloys with transition metals, Mater. Sci. Eng.: A 352 (2003) 100–104.
[5] (a) J.M. Sater, Institute for Defense Analysis, Alexandria, Virginia;
(b) S.C. Jha Marko Materials, Inc., North Billerica, Massachusetts and;
(c) T.H. Sanders J.R., Microstructure and properties of rapidly solidified aluminum-transition metal alloys, Treatise Mater. Sci. Technol. 31 (1989) 409–444.
[6] S. Nayak, M. Wollgarten, J. Banhart, S. Pabi, B. Murty, Nanocomposites and an extremely hard nanocrystalline intermetallic of Al–Fe alloys prepared by mechanical alloying, Mater. Sci. Eng.: A 527 (2010) 2370–2378.
[7] V. Fadeeva, A. Leonov, "Amorphization and crystallization of Al-Fe alloys by mechanical alloying", Mater. Sci. Eng.: A vol. 206 (1996) 90–94.
[8] D. Zhang, G. Adam, B. Ammundsen, Phase formation during mechanical alloying and subsequent low-temperature heat treatment of Al–27.4 at.% Fe–28.7 at.% C powders, J. Alloy. Compd. 340 (2002) 226–230.
[9] T. Sasaki, T. Ohkubo, K. Hono, Microstructure and mechanical properties of bulk nanocrystalline Al–Fe alloy processed by mechanical alloying and spark plasma sintering, Acta Mater. 57 (2009) 3529–3538.
[10] S. Fang, W. Chen, Z. Fu, Microstructure and mechanical properties of twinned $Al_{0.5}CrFeNiCo_{0.3}C_{0.2}$high entropy alloy processed by mechanical alloying and spark plasma sintering, Mater. Des. 54 (2014) 973–979.
[11] L. Lu, M. Lai, Formation of new materials in the solid state by mechanical alloying, Mater. Des. vol. 16 (1995) 33–39.
[12] C. Suryanarayana, F. Froes, Nanocrystalline titanium-magnesium alloys through mechanical alloying, J. Mater. Res. 5 (1990) 1880–1886.
[13] C. Suryanarayana, Mechanical alloying and milling, Prog. Mater. Sci. 46 (2001) 1–184.
[14] V. Tcherdyntsev, S. Kaloshkin, D. Gunderov, E. Afonina, I. Brodova, V. Stolyarov, Y.V. Baldokhin, E. Shelekhov, I. Tomilin, Phase composition and microhardness of rapidly quenched Al–Fe alloys after high pressure torsion deformation, Mater. Sci. Eng.: A vol. 375 (2004) 888–893.
[15] M. Rajabi, M. Vahidi, A. Simchi, P. Davami, Effect of rapid solidification on the microstructure and mechanical properties of hot-pressed Al–20Si–5Fe alloys, Mater. Charact. 60 (2009) 1370–1381.
[16] L. Lu, Y. Zhang, Influence of process control agent on interdiffusion between Al and Mg during mechanical alloying, J. Alloy. Compd. 290 (1999) 279–283.
[17] J.S. Wang, S.G. Donnelly, P. Godavarti, C.C. Koch, Microstructures and mechanical behavior of mechanically alloyed nickel aluminide, Int. J. powder Metall. 24 (1986) 315–325 1988.
[18] A.S. Khan, B. Farrokh, L. Takacs, Effect of grain refinement on mechanical properties of ball-milled bulk aluminum, Mater. Sci. Eng.: A 489 (2008) 77–84.
[19] A. Patterson, The Scherrer formula for X-ray particle size determination, Phys. Rev. 56 (1939) 978.
[20] M. Fine, Y. Kim, W. Griffith, Dispersion Strengthened Aluminium Alloys, TMS, Warrendale, PA, USA (1988), p. 103.
[21] D.K. Mukhopadhyay, C. Suryanarayana, F.H. (SAM) Froes, Structural evolution in mechanically alloyed Al-Fe powders, Metall. Mater. Trans. A 26A (1995) 1939–1946.
[22] S.S. Nayak, B.S. Murty, S.K. Pabi, Structure of nanocomposites of Al–Fe alloys prepared by mechanical alloying and rapid solidification processing, Bull. Mater. Sci. 31 (3) (2008) 449–454.
[23] A.V. Dobromyslov, N.I. Taluts, V.P. Pilyugin, T.P. Tolmachev, Mechanical alloying of Al–Fe alloys using severe deformation by high-pressure torsion, Phys. Met. Met. 116 (9) (2015) 942–950.
[24] X.P. Niu, L. Froyen, L. Delaey, Effect of Fe content on the mechanical alloying and mechanical properties of Al–Fe alloys, J. Mater. Sci. 29 (1994) 3724–3732.